Baosteel Technical Research
Volume 19(End), Number 4, December 2025, Page 1

Titanium

Study of the microstructure and mechanical properties of narrow-gap TIG welded joints using novel low-cost Ti6411 titanium alloy

LANG Yongkun[1], *YANG Shengli*[1),2)], *GAO Fuyang*[1),2)], *JIANG Peng*[1),2)] *and JIANG Tiantian*[1)]

1) Luoyang Ship Material Research Institute, Luoyang 471039, Henan, China;
2) National Key Laboratory of Marine Corrosion and Protection, Luoyang 471039, Henan, China

Abstract: Narrow-gap TIG welding experiments were conducted on novel low-cost Ti6411 titanium alloy, and the microstructure characteristics and mechanical properties of the welded joints were systematically explored. A high-quality weld surface was attained, and there were no defects (such as pores and cracks) inside the weld, thereby meeting the requirements of Class I weld standards. The microstructures of the weld center, heat-affected zone, and base metal were needle-like α′ martensite microstructure, fine (α + β) microstructure, and lath-shaped α and β transformed structures, respectively. The microhardness distribution of the welded joint presented an M-shaped pattern. Due to the fine-grain strengthening and phase-interface strengthening effects, the highest and the lowest hardness occurred in the heat-affected zone (418(HV)) and weld center (294(HV)), and the latter was related to the coarse columnar crystal structure. Tensile tests indicated that the yield strength of the welded joint (804–829 MPa) was close to that of the base metal (808–814 MPa), but elongation (6.5%–8.0%) was significantly lower than that of the base metal (14%–15.5%). The fracture surface showed mixed characteristics of fine dimples and brittle fractures. Impact tests revealed that the impact energy of the weld center (49–65 J) was better than that of the base metal (34–40 J), while the impact toughness of the heat-affected zone fluctuated greatly (27–50 J) due to its uneven microstructure. These results show that Ti6411 alloy has good weldability, but it is necessary to improve the weld plasticity and heat-affected zone toughness by optimizing the welding process.

Key words: low-cost titanium alloy; TIG welding; microstructure; mechanical properties

doi: 10.3969/j.issn.1674-3458.2025.04.001

1 Introduction

Titanium alloys are widely utilized in the aerospace and marine industries due to their low density, high specific strength, and excellent corrosion resistance. Nevertheless, compared with steel and aluminum alloys, their relatively high cost has emerged as a major obstacle to further development. Therefore, research on low-cost titanium alloys is of substantial importance. Low costs can be achieved by using inexpensive elements to reduce raw material costs and by shortening the manufacturing process to lower production costs[1-2]. Ti6411, a new low-cost titanium alloy, has been developed from widely used and low-cost TC4 titanium alloy scrap. The alloy comprises a Cr–Fe master alloy and is designed using d-electron theory. It has a phase ideal cluster structure and is subsequently prepared via a direct melting-rolling-heat treatment process employing the dual-melting technologies of vacuum arc remelting and electron beam cold hearth melting.

TIG welding is a stable welding process, which has the advantages of beautiful welding appearance, good comprehensive mechanical properties after welding, simple operation, and easy automation; as such, it is a common and widely utilized welding method employed with titanium alloys. However,

Corresponding author: YANG Shengli; **E-mail**: yangshengli37@126.com

when the thickness of the test plate increases, traditional TIG welding is no longer considered suitable in terms of welding efficiency, consumption of the welding filler metal, and welding costs. The narrow-gap and small-groove welding concept can not only address the cost issues of conducting traditional TIG welding in thick plate welding but also ensure that the number of welding passes from top to bottom remains nearly identical, leading to a high consistent weld width. YANG et al.[3] summarized the development status, process principles, characteristics, application scopes, and key technical challenges involved in employing commonly used large-thickness titanium alloy welding methods, which include narrow-gap TIG welding, MIG welding, narrow-gap laser welding with wire filling, narrow-gap submerged arc welding, narrow-gap hybrid welding, vacuum electron beam welding, and ultra-narrow-gap welding. HU et al.[4] found that using an external magnetic field to achieve periodic arc oscillation can effectively control the heat input distribution and improve the problem of poor side-wall fusion. Compared with other narrow-gap welding technologies, a more uniform weld microstructure and excellent joint mechanical properties can be obtained through magnetically controlled narrow-gap TIG welding. Following this process, there is a large tensile stress on the joint surface, and an appropriate heat treatment can be applied to effectively reduce the residual stress of the joint. The microstructure and mechanical properties of titanium alloy joints using the narrow-gap TIG welding process have been extensively analyzed[5-11].

Narrow-gap TIG welding experiments were conducted on a low-cost Ti6411 titanium alloy in this study. The microstructure and basic mechanical properties of the welded joints of this titanium alloy were analyzed, and the results provide a foundation for developing low-cost titanium alloys and accelerating their popularization and application.

2 Experimental materials and methods

The chemical composition of the Ti6411 base metal is presented in Table 1. As shown in Fig. 1, the microstructure of the base metal is predominantly composed of lath-shaped α phase and β transformed structure, exhibiting a relatively uniform overall distribution but with certain orientation differences. The addition of Fe and Cr further stabilizes the β phase and influences the phase transformation temperature and microstructure morphology, leading to precipitation of the α phase in the form of lath from the β phase during cooling and the formation of an interlaced lath structure.

Table 1 Chemical composition of the base metal %

w(Fe)	w(Al)	w(V)	w(Mo)	w(Cr)	w(C)	w(Ti)
0.900	5.820	4.110	0.018	0.860	0.012	Balance

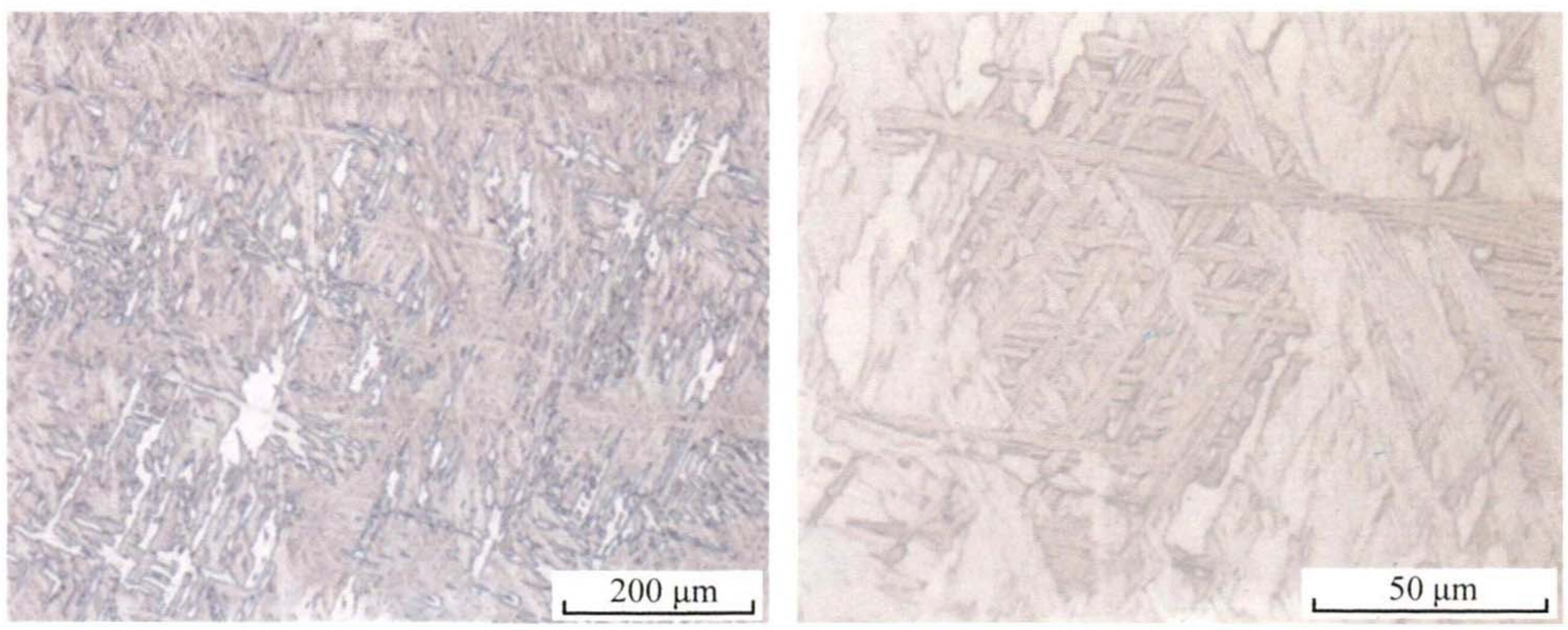

Fig. 1 Microstructure of the base metal

The welded test plate measured 350 mm × 100 mm with a thickness of 35 mm. It featured a double-U groove with a 2 mm blunt edge, as depicted in Fig. 2. The narrow-gap TIG welding method was employed, and a TC3 welding wire was selected for the welding experiment. The welding process parameters are

listed in Table 2. Prior to welding, the surface of the test plate was cleaned to ensure the absence of oxidation, inclusions, or oil contamination. Following the application of argon gas protection, root welding, double-sided filling welding, and cap welding were conducted in sequence. During filling welding, the thickness of each layer of the deposited metal was not less than 3 mm, as required, and the interlayer temperature was maintained below 100 ℃.

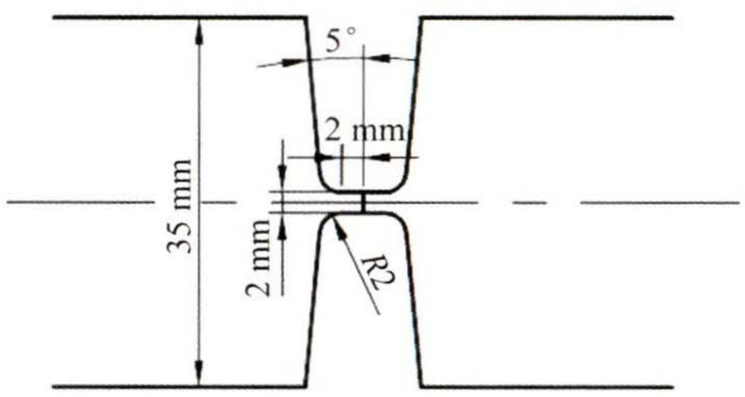

Fig. 2 Schematic diagram of the groove

Table 2 Parameters of narrow-gap TIG welding process

Root current/A	Filling current/A	Cap current/A	Welding speed/(mm · min^{-1})
160–180	200–220	200–220	100–200

After welding, the test plate underwent non-destructive testing to evaluate the welding quality of the weld. Upon meeting the qualification requirements, wire-cutting equipment was utilized to prepare a sample, and metallographic samples of the weld cross-section were extracted perpendicular to the welding direction. Following grinding with sandpaper and polishing with a polishing machine, chemical corrosion was performed using a corrosive solution (HF, HNO_2, H_2O). The microstructure of the welded joint was then observed using an OLYMPUS GX71 metallographic microscope, and the microhardness of the welded joint was measured from one side of the base metal to the other using a Wilson VH3300 microhardness tester. Three parallel tensile and impact samples were taken from the weld filling position. Tensile samples were processed according to Fig. 3(a), and room-temperature tensile tests were conducted using an INSTRON 5985-250kN material testing machine. Impact samples were processed according to Fig. 3(b), and room-temperature impact tests were conducted using a ZBC2602-C pendulum impact testing machine. Finally, the fracture surfaces of the tensile and impact samples were observed using a Quanta 650 scanning electron microscope.

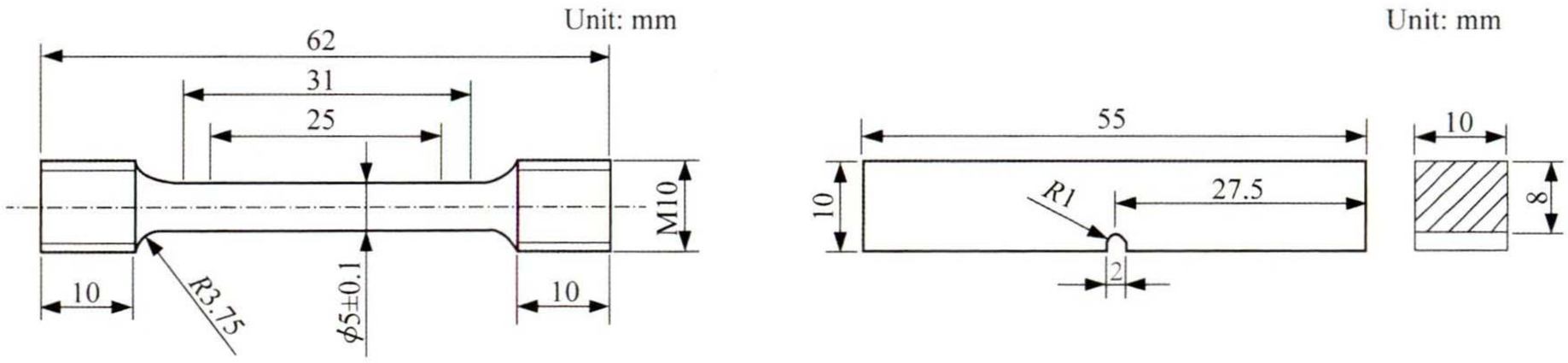

(a) Tensile sample (b) Impact sample

Fig. 3 Schematic diagrams of standard samples

3 Results and analysis

3.1 Macroscopic morphology and quality of weld

The macroscopic morphology of the weld of the Ti6411 novel low-cost titanium alloy after welding is shown in Fig. 4. The weld surface is seen to be light yellow in color; this is indicative of a low oxidation degree, and it does not reduce the performance of the titanium alloy. Following welding, penetrant testing was conducted on the weld, and the test results revealed no cracks on the weld surface, complying with the requirements of Class I in NB/T 47013.5–2015. X-ray testing was also performed on the weld, and the results demonstrated that internal fusion was complete, with no pores, cracks, or inclusions, thereby meeting the requirements of Class I in NB/T 47013.2–2015. This demonstrated that the Ti6411 low-cost

titanium alloy possessed good weldability.

Fig. 4 Macroscopic morphology of the weld

3.2 Microstructure of the welded joint

The macroscopic morphology of the welded joint of the Ti6411 novel low-cost titanium alloy is shown in Fig. 5. The welded joint comprised the weld metal (WM), heat-affected zone (HAZ), and base metal (BM). The narrow-gap TIG weld was formed through the stacking of multiple weld passes. The HAZ was relatively wide, and the weld joint consisted of a substantial amount of columnar crystal tissue (filling position) and a minor amount of equiaxed crystal tissue (root position). This phenomenon occurred because during root welding, the molten pool was situated in the center of the plate, and heat dissipation occurred relatively uniformly. When subsequent filling welding was conducted, the root weld underwent reheating, which induced phase transformation and recrystallization and led to the disappearance of internal columnar crystals and the formation of equiaxed crystal tissue. During filling welding, with a gradual rise in the molten pool, the heat was predominantly dissipated to the surface of the test plate perpendicular to the groove direction, thereby forming columnar crystal tissue.

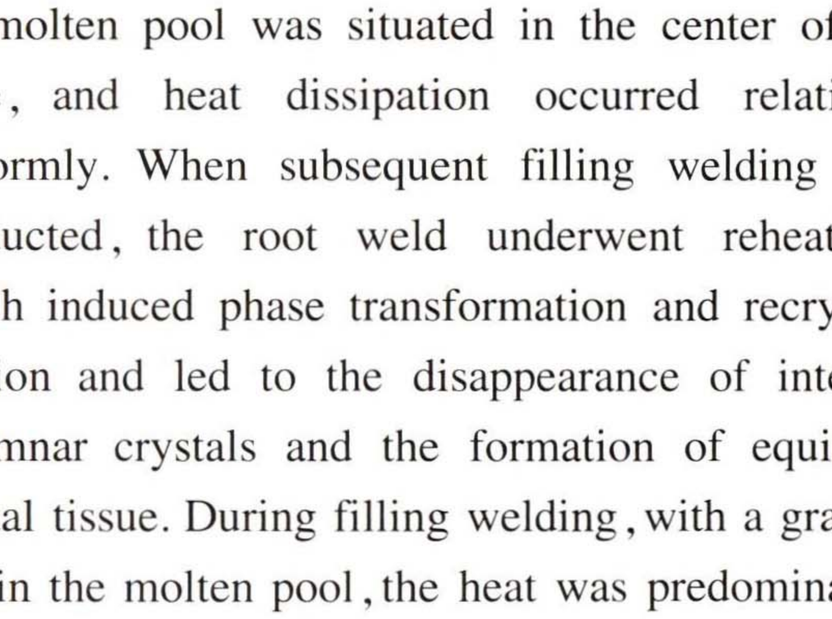

Fig. 5 Macroscopic morphology of the welded joint

The microstructure of the filling position in the Ti6411 novel low-cost titanium alloy is shown in Fig. 6. The columnar crystal morphology at the weld center was obvious, such that complete grains were not seen. The microstructure was predominantly composed of needle-like α' martensite. Owing to the relatively rapid cooling rate at the weld center during narrow-gap TIG welding, the high-temperature β phase lacked sufficient time to decompose into the equilibrium ($\alpha + \beta$) tissue, leading to the formation of metastable α' martensite. The presence of columnar crystals also indicated that this region underwent a rapid solidification process during welding. The microstructure of the HAZ lay between that of the BM and the weld center. However, unlike the weld center, no obvious columnar crystals are present, but a certain grain coarsening tendency was evident. The fine α phase was observed in the microstructure, and this was finer and more diffusely distributed than that in the BM. This is because the HAZ was subjected to the welding thermal cycle, although its peak temperature was lower than that at the weld center, and the cooling rate was relatively slower, resulting in a certain degree of grain coarsening without the formation of directional columnar crystals. Simultaneously, the β phase partially decomposed, precipitating the fine α phase, but due to the relatively fast cooling rate, it did not have sufficient time to grow into the coarse lath-shaped α phase similar to that in the BM.

Significant differences were observed between the columnar crystal morphology and α' phase microstructure at the weld center and those of the BM. The lath-shaped α phase in the BM had an equilibrium microstructure, whereas the metastable α' phase was formed at the weld center due to rapid cooling, and the crystal growth morphology exhibited directional columnar crystals under the influence of welding heat flow. This resulted in relatively high hardness at the weld center, albeit a likely decrease in toughness, exhibiting obvious differences from the comprehensive mechanical properties of the BM.

Although some of the BM characteristics were retained in the HAZ microstructure, changes in grain size and α phase morphology were evident. Compared with the coarse lath-shaped α phase in the BM, the α phase in the HAZ was finer, and a certain grain coarsening tendency was present. This indicated that the HAZ microstructure was in a partially recrystallized state due to the welding thermal cycle, and its mechanical properties (such as strength and toughness) also lay between those of the BM and the weld center, presenting a certain performance gradient, which is consistent with the results of other related studies[12-13].

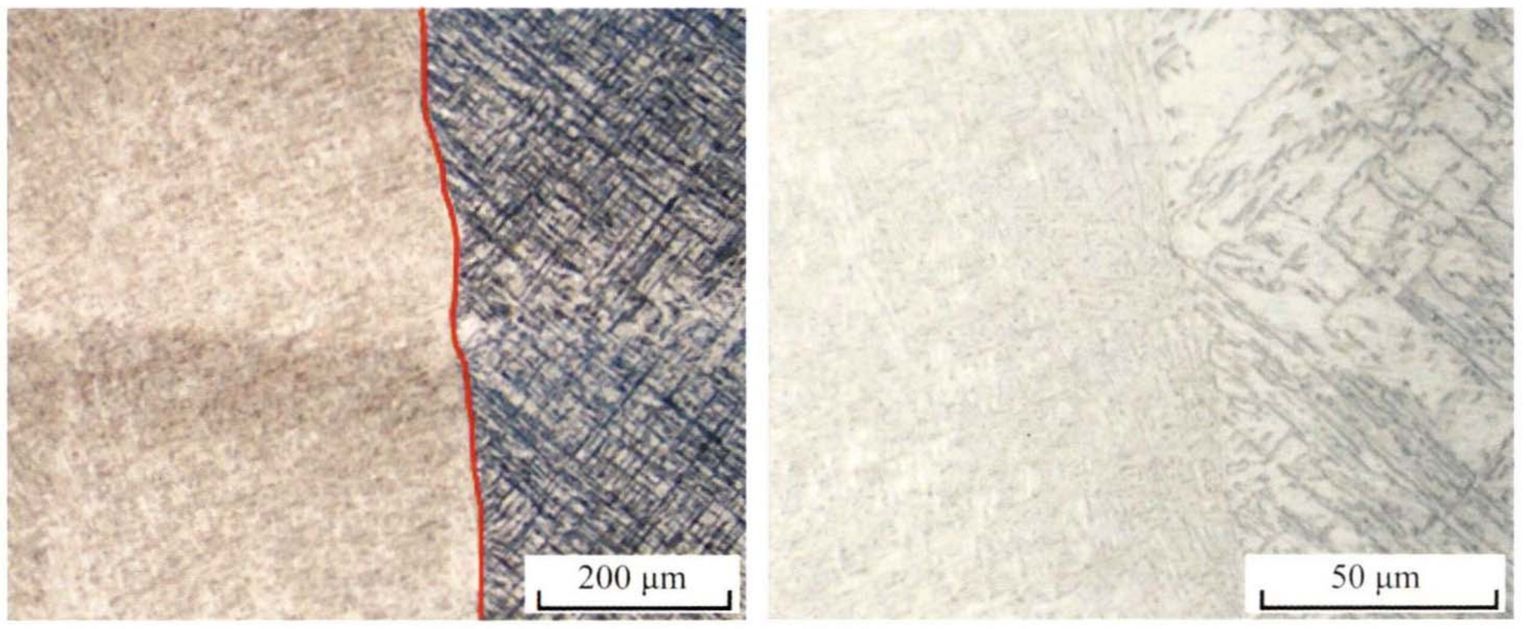

(a) Weld center

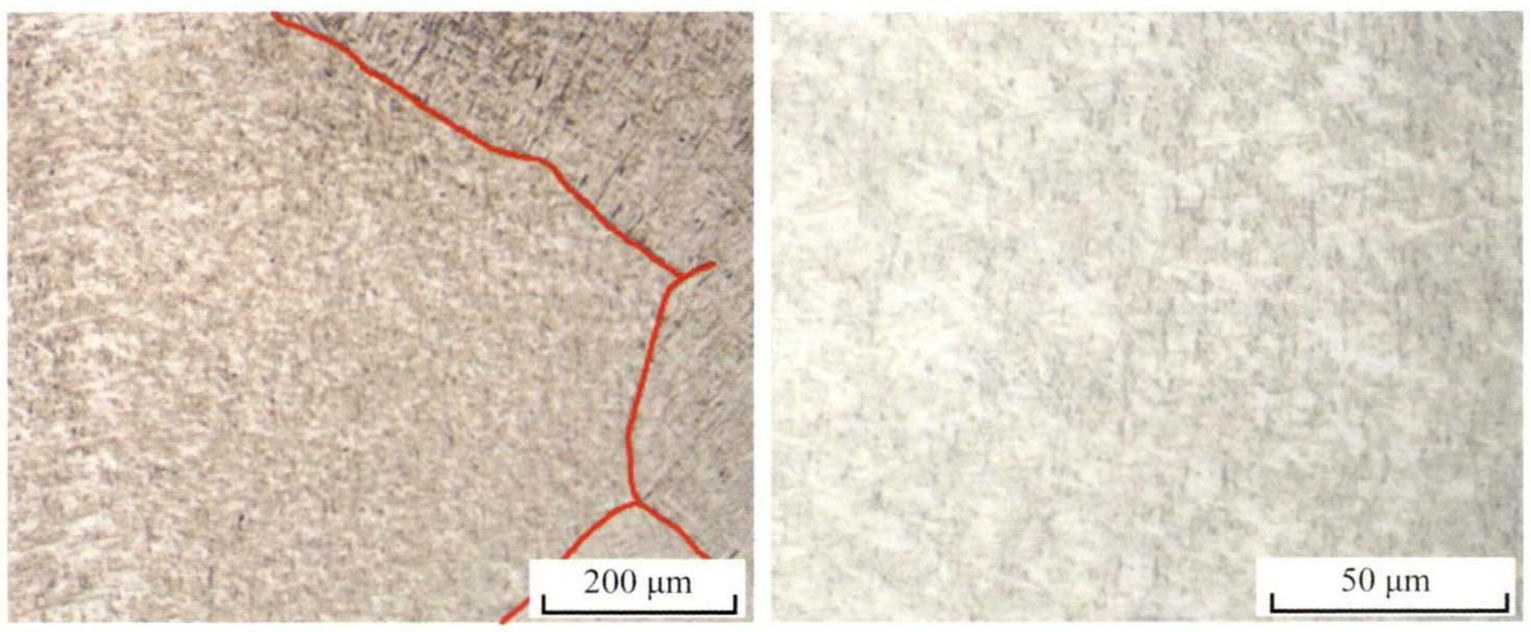

(b) HAZ

Fig. 6 Microstructure of the filling position

3.3 Microhardness of the welded joint

The microhardness test results of the welded joint of the Ti6411 novel low-cost titanium alloy are shown in Fig. 7. The microhardness distribution of the welded joint presented an M-shaped pattern. The maximum and minimum microhardness (HV) at the cap position, filling position, and root position reached 418 and 299, 405 and 294, and 410 and 334, respectively. All maximum and minimum hardness values were located in the HAZ and weld center, respectively. The hardness of the BM lay between that of the HAZ and the weld center.

The microstructure of the weld center was dominated by a needle-like α′ phase, which inherently possessed relatively high hardness. Nevertheless, during the welding process, due to the directional growth of columnar crystals in the weld area, relatively coarse α′ phase columnar crystals with a small number of grain boundaries were formed upon cooling. The hindrance of grain boundaries to dislocation movement was reduced, and the uniformity of the coarse columnar crystal structure was relatively poor, leading to relatively low overall hardness. Additionally, the single α′ phase microstructure lacked the synergistic strengthening effect of phase interfaces, further causing the weld area to become the region with the lowest hardness. Fine α phase precipitates were contained in the HAZ

microstructure, and due to the welding thermal cycle, this region underwent a partial recrystallization process, forming fine ($\alpha+\beta$) tissue. Here, the fine-grain strengthening mechanism played a key role: fine grains increased the number of grain boundaries, making it more likely for the dislocation movement to be hindered by grain boundaries, thus significantly enhancing the material's hardness. Meanwhile, the phase interfaces between the α phase and the β phase also increased the resistance to dislocation movement, further strengthening the hardness of this region and making it the region with the highest hardness. The BM microstructure was composed of lath-shaped α phase and β transformed tissue, with relatively coarse and evenly distributed α phase laths. Its microstructural state lay between the coarse α' phase at the weld center and the fine ($\alpha+\beta$) tissue in the HAZ. Owing to the absence of fine-grain strengthening and the high dispersion of phase interfaces, the hardness of the BM was lower than that of the HAZ but higher than that of the weld center. A large proportion of the BM was occupied by the root weld passes, which increased the microhardness at the weld position, and similar results have been obtained in other studies[13-15]. Therefore, the microhardness at the root position was higher than that at the filling and cap positions.

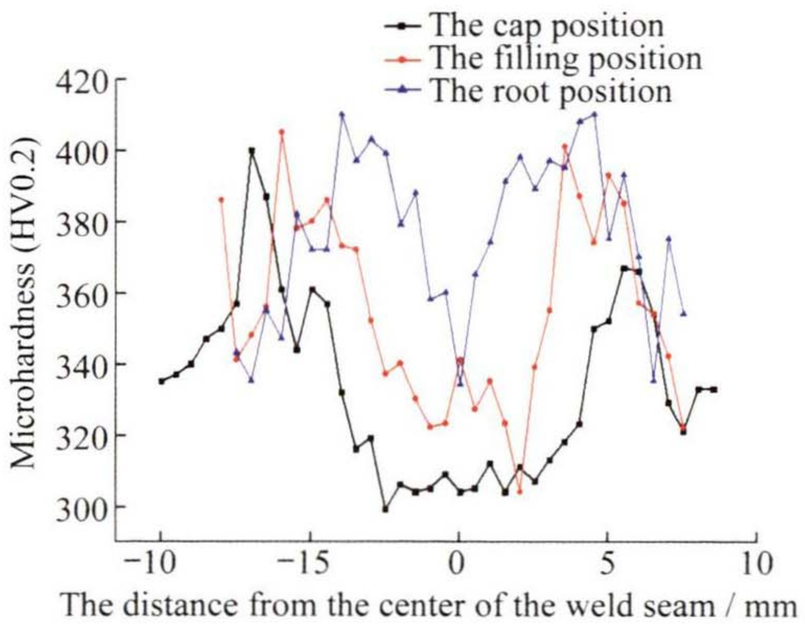

Fig. 7 Microhardness of the welded joint

3.4 Tensile properties of the welded joint

Table 3 illustrates the room-temperature tensile properties of the welded joint of the Ti6411 novel low-cost titanium alloy. The yield and tensile strength of the welded joint were 804−829 MPa and 914−928 MPa, respectively, while those of the BM were 808−814 MPa and 944−945 MPa. The yield strength of the welded joint was close to that of the BM, indicating that the strength loss of the welded joint was relatively small. This phenomenon can be attributed to the high strength of the α' phase formed in the weld. The elongation of the welded joint and the BM were 6.5%−8.0% and 14.0%−15.5%, respectively. The elongation of the welded joint was significantly lower than that of the BM, primarily due to the presence of the needle-like α' phase in the weld microstructure. The metastable structure of this phase led to insufficient toughness, limited dislocation slip, and a reduced plastic deformation ability.

Table 3 Room-temperature tensile properties of the welded joint

Region	Yield strength ($R_{p0.2}$)/MPa	Tensile strength (R_m)/MPa	Elongation (A)/%	Fracture position
Welded joint	810,804, 829,826	928,917, 924,914	6.5,8.0, 7.5,8.0	Weld
BM	814,808	945,944	15.5,14.0	–

The fracture surface of the tensile sample from the Ti6411 novel low-cost titanium alloy welded joint is shown in Fig. 8. The fracture surface exhibited a certain degree of undulation, indicating the complexity of the fracture process, which may have been associated with multiple crack initiation sources. A large number of fine dimples were observed on the fracture surface, suggesting that the fracture process involved ductile fracture characteristics[16-18]. However, the dimples were small in size and shallow in depth, reflecting a limited plastic deformation capacity. When combined with the tensile data, this phenomenon was attributed to the brittle tendency of the α' phase in the weld. Although dimples were present, the full slip of dislocations and the expansion of dimples were limited by the needle-like structure of the α' phase, leading to a lower elongation compared to the BM.

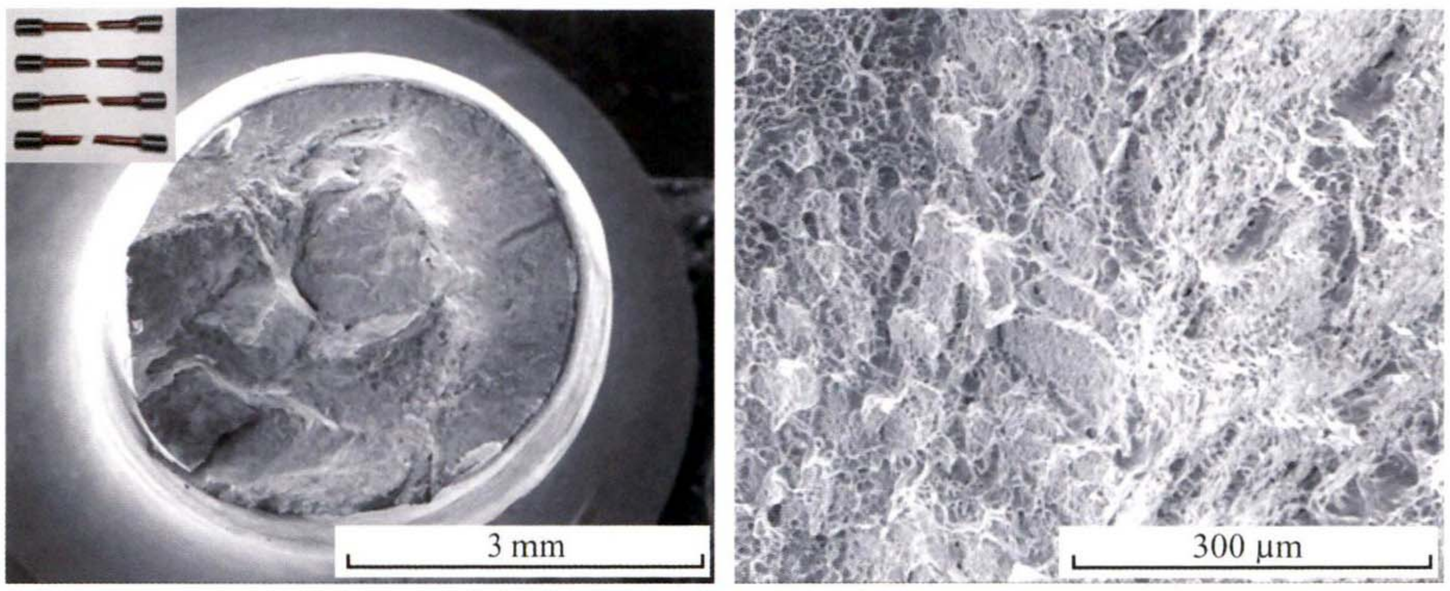

Fig. 8 Fracture surface of the tensile sample of the welded joint

3.5 Impact properties of the welded joint

Table 4 displays the room-temperature impact properties of the Ti6411 novel low-cost titanium alloy welded joint. The impact energy at the weld center was 49–65 J, with the values relatively high and concentrated, indicating that under the impact load, the weld absorbs more energy and has good impact resistance. The impact energy in the HAZ was 27 – 50 J, with a large fluctuation range, reflecting that impact toughness was significantly affected by the uneven microstructure in this region, with some areas exhibiting poor impact resistance. The impact energy of the BM was 34–40 J, demonstrating a relatively stable performance, although the results were overall lower than those of the weld. This trend is consistent with results from related research[13,16-18].

Table 4 Room-temperature impact properties of the welded joint Unit: J

Region	Impact energy (KU_2)
Weld center	58,63,65,50,49,57
HAZ	27,31,46,50,28,31
BM	40,36,34

Scanning electron microscope images of fracture surfaces of the impact samples from the Ti6411 novel low-cost titanium alloy welded joint are shown in Fig. 9. The fracture surface of the weld center exhibited an undulating shape as a whole. At high magnification, a large number of dense and deep dimples were evident, indicating that the fracture was mainly of a ductile nature. MOHANDAS et al.[19], YU et al.[20], and GAO et al.[21] found that phase boundaries such as α/β and α/α' hinder crack propagation or cause cracks to change their propagation direction at the phase boundaries, which is beneficial to improving impact toughness[22-24]. During the impact process, dislocation movement occurred between the needle-like α' phase structures, causing local plastic deformation, the formation of dimples, and energy absorption, thus resulting in higher impact energy. Due to the welding thermal cycle, the HAZ had an uneven microstructure, featuring fine α phase precipitates and potential local grain coarsening or tissue defects (such as residual stress concentration areas). The fracture surface morphology was complex, with fewer dimples and some cleavage characteristics (e. g., river-like patterns) revealed at high magnification, indicating a tendency toward brittle fracture. While the fine α phase can provide a certain level of toughness, forming a small number of dimples, in locally coarsened grain or defect areas, cleavage fracture (brittle fracture) is likely to occur due to weak grain boundary bonding or stress concentration. This results in large fluctuations in impact energy and a mixed ductile-brittle fracture characteristic[25]. The fracture surface of the BM was relatively flat, with evenly distributed dimples observed at high magnification, although they were smaller than those in the weld and fewer in number[26-27]. During impact, the lath-shaped α phase microstructure restricted dislocation

slip via the lath interfaces, leading to less plastic deformation and weaker energy absorption ability than the weld; therefore, the impact energy of the BM was lower than that of the weld. However, due to its good microstructure uniformity and absence of obvious defect areas, the impact toughness of the BM was stable, primarily exhibiting ductile fracture with limited plastic deformation.

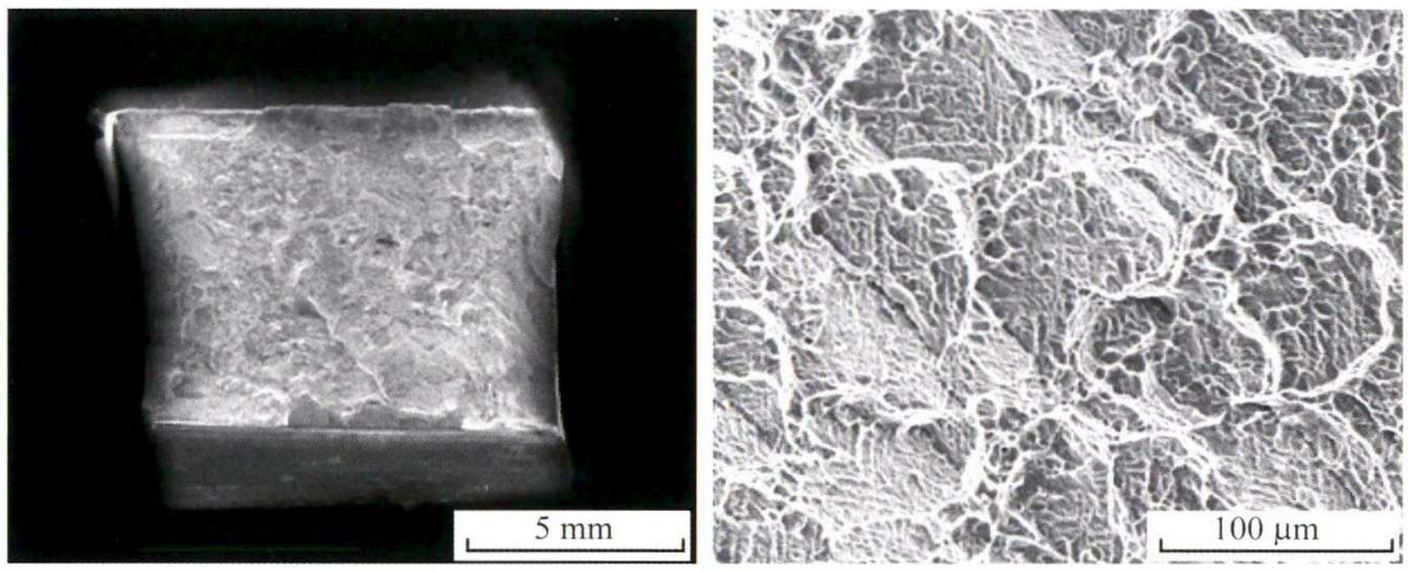

(a) Weld center

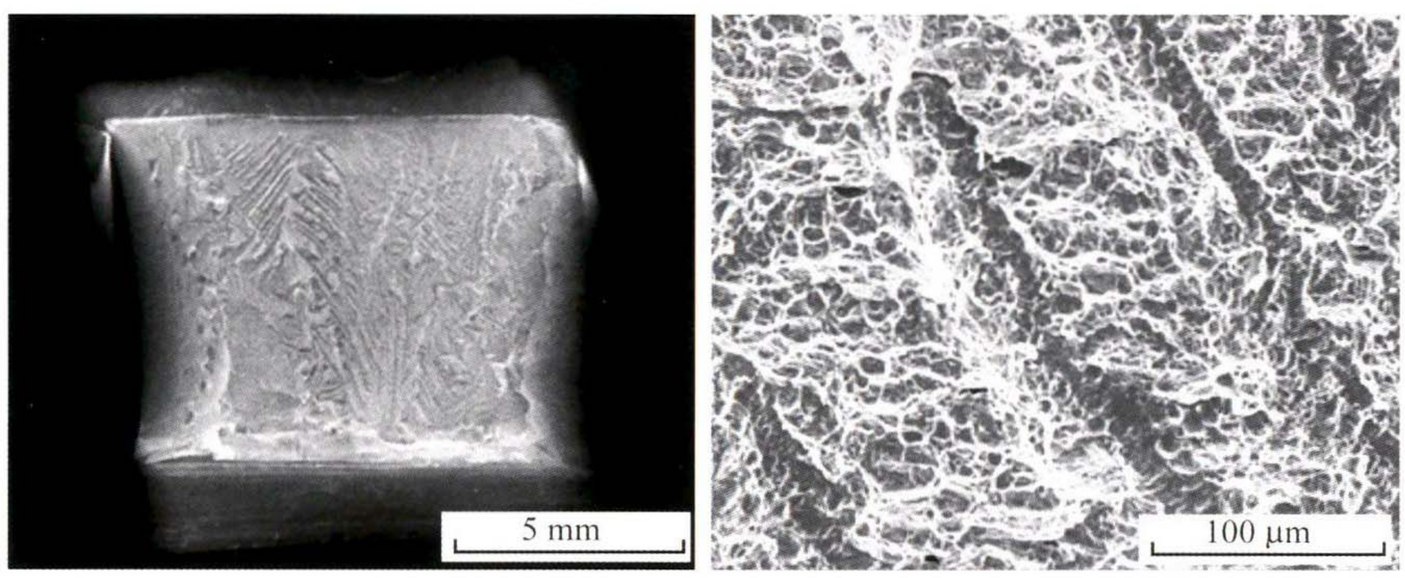

(b) HAZ

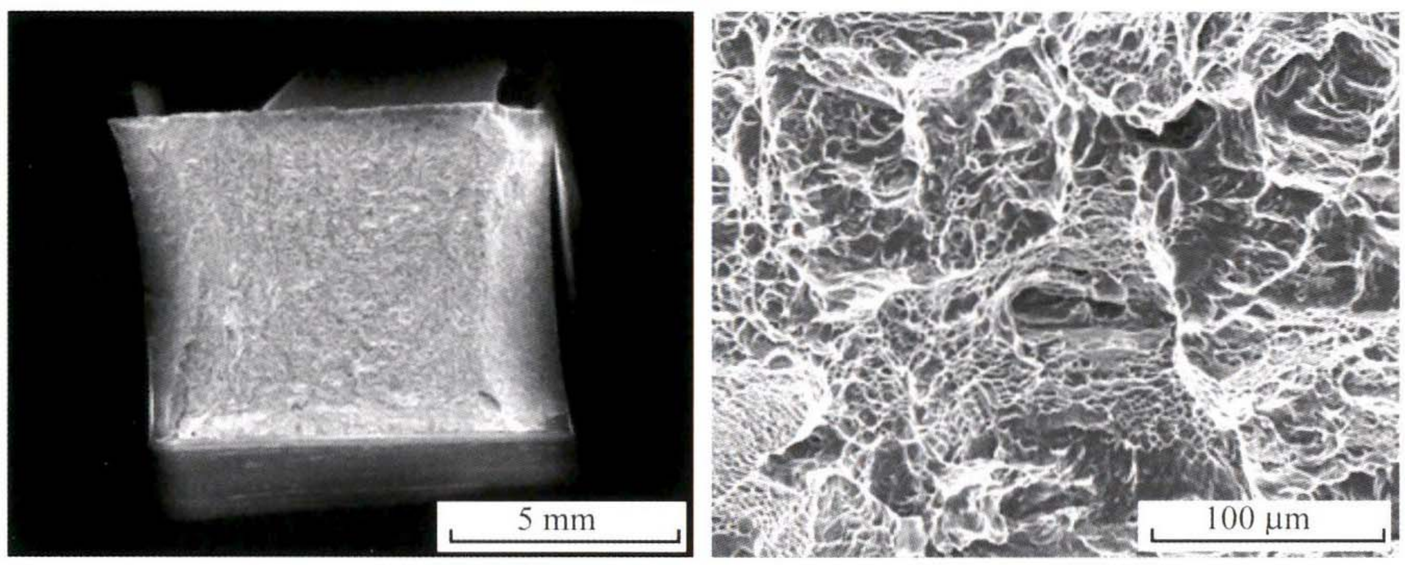

(c) BM

Fig. 9 Fracture surfaces of impact samples from the welded joint

4 Conclusions

(1) The weld surface quality of the Ti6411 novel low-cost titanium alloy was excellent, and the internal weld areas demonstrated sound metallurgical bonding. No welding defects (such as pores, cracks, inclusions, or abnormal microstructures) were detected, indicating excellent weldability.

(2) The microhardness distribution of the Ti6411 novel low-cost titanium alloy welded joint exhibited an M-shaped pattern. The weld center microstructure consisted of a needle-like α' phase, which inherently possessed relatively high hardness. However, due to the directional growth of columnar crystals in the weld area during welding, the α' phase columnar crystals formed upon cooling were relatively coarse, with a reduced number of grain boundaries. The hindrance of grain boundaries to dislocation movement was diminished, resulting in relatively low overall hardness. The HAZ microstructure

contained fine α phase precipitates, and through the welding thermal cycle, this region underwent partial recrystallization, forming fine (α + β) tissue. Simultaneously, phase interfaces between α and β phases enhanced resistance to dislocation movement, further strengthening this region and making it the area with the highest hardness.

(3) The welded joint of the Ti6411 novel low-cost titanium alloy displayed a yield strength of 804–829 MPa, a tensile strength of 914–928 MPa, and an elongation of 6.5%–8.0%. While its strength was comparable to that of the BM, its plasticity was relatively poor. The impact energy at the weld center ranged from 49 to 65 J, with relatively high and concentrated values, indicating that the weld could absorb substantial energy under impact loading and that it possessed good impact resistance. The impact energy in the HAZ ranged from 27 to 50 J, with significant fluctuations, reflecting that the uneven microstructure in this region significantly influenced impact toughness, with some areas exhibiting poor impact resistance. In the future, the welding process (such as controlling the cooling rate and adjusting heat treatment parameters) can be optimized to refine the weld microstructure and enhance plasticity.

Data availability statement

The raw/processed data that support the findings of this study are available from the corresponding author upon reasonable request.

Acknowledgments

The authors acknowledge the financial support from the the National Key R&D Program of China (No. 2022YFB3705605).

References

[1] FENG Q Y, TONG X W, WANG J, et al. Status quo and development tendency on the research of low cost titanium alloy[J]. Materials Review, 2017, 31(5): 128-134.

[2] XIN S W, LIU X H, ZHANG S Y, et al. An overview on research and development of low cost titanium alloys[J]. Rare Metal Materials and Engineering, 2023, 52(11): 3971-3980.

[3] YANG X G, LIAO Z Q, LIU X L, et al. Current status and development of welding technology of large thickness titanium alloy[J]. Welding Technology, 2024, 53(2): 5-11.

[4] HU J L, ZENG C Y, YU C, et al. Progress in magnetically-controlled narrow-gap TIG welding of thick-plate titanium alloys[J]. Journal of Netshape Forming Engineering, 2020, 12(4): 10-20.

[5] CONG C M, ZENG C Y, ZHANG Y P, et al. Microstructure and mechanical properties of magnetically controlled narrow gap TIG welding joint of titanium alloy thick plate[J]. Hot Working Technology, 2024, 53(13): 24-29.

[6] HU J L, HU Y J, ZENG C Y, et al. Microstructure and mechanical properties of welded joints of TA17 Ti alloy by magnetically controlled narrow-gap TIG welding[J]. Hot Working Technology, 2023, 52(9): 42-46, 50.

[7] CHEN L J, NING H N, ZHANG Z P, et al. High cycle fatigue properties of narrow gap TIG welded joint of thick TC4 titanium alloy plate[J]. Journal of Shenyang University of Technology, 2023, 45(4): 397-402.

[8] SUN Q J, SUN Q, LIU Y B, et al. Microstructure and properties of TA31 alloy magnetically controlled narrow gap TIG welded joint[J]. Development and Application of Materials, 2024, 39(4): 1-9.

[9] AN F P, DENG X H, LIU Q L, et al. Study of narrow gap TIG welding and electron beam welding of thick TA31 alloy[J]. Development and Application of Materials, 2020, 35(5): 81-86.

[10] TIAN X M, WEI N, ZHOU Z B, et al. Study on microstructure and properties of Ti-Al-Fe low cost titanium alloy by TIG welding[J]. Titanium Industry Progress, 2020, 37(5): 23-26.

[11] YANG Q F, ZENG C Y, ZHANG Y P, et al. Effect of large-thickness TC4 titanium alloy narrow gap weld structure on mechanical properties of joints[J]. Electric Welding Machine, 2023, 53(8): 8-15.

[12] GAO F Y, LI P Y, JIANG P, et al. The effect of constraint conditions on microstructure and properties of titanium alloy electron beam welding[J]. Materials Science and Engineering: A, 2018, 721: 117-124.

[13] XIONG J H, LI S K, GAO F Y, et al. Microstructure and mechanical properties of Ti6321 alloy welded joint by GTAW[J]. Materials Science and Engineering: A,

2015,640:419-423.

[14] YU W X, HOU S S, LV Y F, et al. Evolution of microstructure and mechanical properties of vacuum electron beam welded joints in a near beta titanium alloy:influence of heat treatment[J]. Vacuum, 2022, 204:111362.

[15] GAO F Y,CUI Y J,LV Y F,et al. Microstructure and properties of Ti-6Al-4V alloy welded joint by keyhole gas tungsten arc welding[J]. Materials Science and Engineering:A,2021,827:142024.

[16] GAO F Y,GAO Q,JIANG P,et al. Microstructure and mechanical properties of Ti6321 alloy welded joint by EBW[J]. International Journal of Lightweight Materials and Manufacture,2018,1(4):265-269.

[17] HUANG S X, ZHAO Q Y, LIN C, et al. In-situ investigation of tensile behaviors of Ti-6Al alloy with extra low interstitial [J]. Materials Science and Engineering:A,2021,809:140958.

[18] GAO F Y, MU Z Z, MA Z W, et al. Fine microstructure characterization of titanium alloy laser narrow gap welded joint[J]. China Welding,2021,30(3):31-38.

[19] MOHANDAS T, BANERJEE D, KUTUMBA RAO V V. Observations on impact toughness of electron beam welds of an α + β titanium alloy[J]. Materials Science and Engineering:A,1998,254(1/2):147-154.

[20] YU W X, WANG G L, GAO F Y, et al. The microstructure and impact toughness of vacuum electron beam welded joints of a highly alloyed dual phase titanium alloy[J]. Vacuum,2024,221:112877.

[21] GAO F Y,GAO Q,JIANG P,et al. Microstructure and properties of titanium alloy electron beam weldments based on the different heat input conditions of the same line energy[J]. Vacuum,2017,146:136-141.

[22] LEI L, ZHAO Q Y, ZHAO Y Q, et al. Study on the intrinsic factors determining impact toughness of TC21 alloy[J]. Materials Characterization,2021,177:111164.

[23] DUAN Q Q,QU R T,ZHANG P,et al. Intrinsic impact toughness of relatively high strength alloys[J]. Acta Materialia,2018,142:226-235.

[24] GAO F Y,LIAO Z Q,LI W Y,et al. Investigating the impact toughness properties and influential factors of titanium alloy joints[J]. Materials Characterization, 2024,218:114465.

[25] MESHRAM S D, MOHANDAS T. A comparative evaluation of friction and electron beam welds of near-α titanium alloy[J]. Materials & Design, 2010, 31(4): 2245-2252.

[26] BALASUBRAMANIAN M, JAYABALAN V, BALASUBRAMANIAN V. Effect of microstructure on impact toughness of pulsed current GTA welded α-β titanium alloy[J]. Materials Letters,2008,62(6/7):1102-1106.

[27] POLYAKOV A V,RAAB G I,SEMENOVA I P,et al. Mechanical properties of UFG titanium:notched fatigue and impact toughness[J]. Materials Letters,2021,302: 130366.

LANG Yongkun

YANG Shengli

GAO Fuyang

JIANG Peng

JIANG Tiantian